Thermal Stabilities of Brain Spectrin and the Constituent Repeats of Subunits†

Xiuli An,*,‡ Xihui Zhang,‡ Marcela Salomao,‡ Xinhua Guo,‡ Yang Yang,‡ Yu Wu,‡ Walter Gratzer,§ Anthony J. Baines,|| and Narla Mohandas‡

Red Cell Physiology Laboratory, New York Blood Center, New York, New York 10021, King's College London, Randall Center for Molecular Mechanisms of Cell Function, Guy's Campus, London SE1 1UL, U.K., and Department of Biosciences, University of Kent, Canterbury, Kent CT2 7 NJ, U.K.

Received July 6, 2006; Revised Manuscript Received September 6, 2006

ABSTRACT: The different genes that encode mammalian spectrins give rise to proteins differing in their apparent stiffness. To explore this, we have compared the thermal stabilities of the structural repeats of brain spectrin subunits (αII and βII) with those of erythrocyte spectrin (αI and βI). The unfolding transition midpoints (T_m) of the 36 αII- and βII-spectrin repeats extend between 24 and 82 °C, with an average higher by some 10 °C than that of the αI- and βI-spectrin repeats. This difference is reflected in the T_m values of the intact brain and erythrocyte spectrins. Two of three tandem-repeat constructs from brain spectrin exhibited strong cooperative coupling, with elevation of the T_m of the less stable partner corresponding to coupling free energies of approximately −4.4 and −3.5 kcal/mol. The third tandem-repeat construct, by contrast, exhibited negligible cooperativity. Tandem-repeat mutants, in which a part of the "linker" helix that connects the two domains was replaced with a corresponding helical segment from erythroid spectrin, showed only minor perturbation of the thermal melting profiles, without breakdown of cooperativity. Thus, the linker regions, which tolerate few point mutations without loss of cooperative function, have evidently evolved to permit conformational coupling in specified regions. The greater structural stability of the repeats in αII- and βII-spectrin may account, at least in part, for the higher rigidity of brain compared to erythrocyte spectrin.

Spectrin arose in evolution with the metazoa to meet the need for structures that strengthen cell adhesions and stabilize the plasma membrane against the forces of animal movement (*1*). The protein also plays a part in organizing plasma membrane signaling complexes (*1, 2*). Spectrin occurs as an $(\alpha\beta)_2$ tetramer, specialized for cross-linking actin filaments to membrane constituents. Both the α- and β-chains are largely made up of consecutive triple-helical repeating units of ∼106 amino acids (*3, 4*); these act in ensemble as spacers between actin-binding domains in the β-subunits at opposite ends of the tetramers, and some contain binding sites for proteins such as ankyrin or for aminophospholipids (*5, 6*).

The number of spectrin genes increased during evolution with the advent of vertebrates. Invertebrates have one α-spectrin, and one β-spectrin with 16 complete triple-helical repeats and a β_{Heavy} subunit with 30 complete triple helices. Vertebrates have four genes encoding "conventional" β-subunits (βI−IV) that have 16 complete triple-helical modules, and one β_{Heavy} subunit that has 30 triple helices (βV-spectrin) (*1*). Mammals have gained an additional α-spectrin by duplication of the pre-existing α-spectrin gene (*7*). There is now clear evidence of functional specialization of the two mammalian α-spectrins (αI and αII). The αII-spectrins, which are closest in sequence to invertebrate α-spectrins, are abundant in the cells of complex tissues (*8*). They are enriched in such locations as postsynaptic contacts (*9*) (where complexes of signaling molecules reside) and intercalated discs (*10, 11*) (where forces of muscle contraction are transmitted). The importance of spectrin in the resistance of tissues to the forces generated by muscle contraction is evident in all animals; thus, for example, in the worm *Caenorhabditis elegans*, spectrin is required to strengthen adhesion between the body wall and the muscles beneath it (*12, 13*). By contrast, αI-spectrin is abundant in enucleate red blood cells, where it imparts to the membrane the elasticity needed to survive the rigors of circulation (*7, 14, 15*).

The functional distinction between the spectrins of mammalian tissue and erythrocyte is reflected in their physical properties. Spectrin purified from brain (comprising mainly αII and βII polypeptides, also known as fodrin) has a stiffer and straighter appearance in the electron microscope than the erythrocyte (αIβI) spectrin (*16*−*19*), and this difference is also reflected in their hydrodynamic properties (*16, 19*). It might be suggested that the "floppier" appearance of erythrocyte spectrin reflects its adaptation to the requirement for membrane elasticity.

Some 80−90% of each spectrin polypeptide is folded into the sequential triple-helical modules, so it might be supposed that structural and functional differences between the proteins have a counterpart in the properties of their constituent

† This work was supported in part by NIH Grants DK 26263, DK 32094, and HL31579.

* To whom correspondence should be addressed: Red Cell Physiology Laboratory, 310 E. 67th St., New York, NY10021. Telephone: (212) 570-3247. Fax: (212) 570-3195. E-mail: xan@nybloodcenter.org.

‡ New York Blood Center.

§ King's College London.

|| University of Kent.

10.1021/bi061368x CCC: $33.50
Published on Web 10/17/2006

Table 1: Information about αII- and βII-Spectrin Single Repeats[a]

name	amino acids	nucleotides	name	amino acids	nucleotides
αIIR1	39−154	115−462	βIIR1	284−422	850−1266
αIIR2	145−260	433−780	βIIR2	418−533	1252−1599
αIIR3	251−366	751−1098	βIIR3	524−643	1570−1929
αIIR4	357−472	1069−1416	βIIR4	634−749	1900−2247
αIIR5	463−578	1387−1734	βIIR5	740−854	2218−2562
αIIR6	569−683	1705−2049	βIIR6	845−960	2533−2880
αIIR7	674−789	2020−2367	βIIR7	951−1067	2851−3201
αIIR8	780−895	2338−2685	βIIR8	1058−1174	3172−3522
αIIR9−10	886−1096	2656−3283	βIIR9	1165−1280	3493−3840
αIIR11	1087−1238	3265−3705	βIIR10	1271−1385	3811−4155
αIIR12	1229−1344	3685−4032	βIIR11	1376−1490	4126−4470
αIIR13	1335−1450	4003−4350	βIIR12	1481−1597	4441−4791
αIIR14	1441−1556	4321−4668	βIIR13	1588−1703	4762−5109
αIIR15	1547−1663	4639−4989	βIIR14	1694−1810	5080−5430
αIIR16	1654−1769	4960−5307	βIIR15	1801−1916	5401−5748
αIIR17	1760−1875	5278−5625	βIIR16	1907−2022	5719−6066
αIIR18	1866−1981	5596−5943			
αIIR19	1972−2088	5914−6264			
αIIR20	2079−2202	6235−6606			
αIIR21	2193−2317	6577−6951			

[a] The boundaries of all repeats were defined by the SMART database (http://smart.embl.heidelberg.de/) with the exception that five amino acides are extended at both the N-terminus and the C-terminus to ensure proper folding. The six N-terminal amino acids are from vector pGEX-4T-2.

domains. Having previously found that the repeating units of αI- and βI-spectrin vary widely in their thermostabilities (*20*), we were prompted to examine those of αII- and βII-spectrins to investigate the basis of the differences in the gross characteristics of the intact proteins. We have accordingly determined the thermal unfolding properties of each repeat of αII- and βII-spectrin, as well as some constructs comprising selected tandem pairs of repeats, and some with mutations in the single α-helix uniting them.

EXPERIMENTAL PROCEDURES

Materials. Pig brain was purchased from Pel-Freez Biologicals (Rogers, AR). Human brain whole marathon-ready cDNA was from Clontech (Mountain View, CA). Sephacryl S-500HR, pGEX-4T-2 vector, and glutathione−Sepharose 4B were from Amersham Biosciences (Piscataway, NJ). Protease inhibitor cocktail sets II and III were from Calbiochem (San Diego, CA). pET-31b(+) vector and nickel resin were from Novagen (Madison, WI). The QuickChange site-directed mutagenesis kit and BL21(DE3) bacteria were from Stratagene (La Jolla, CA). Restriction enzymes were from New England BioLabs (Beverly, MA), reduced-form glutathione, thrombin, IPTG, DFP, and PMSF from Sigma (St. Louis, MO), and SDS−PAGE and electrophoresis reagents from Bio-Rad (Hercules, CA), and GelCode staining reagent was from Pierce Biotechnology, Inc. (Rockford, IL). Human erythrocyte and pig brain spectrins were purified by the methods of Tyler et al. (*21*) and Davis and Bennett (*19*), respectively.

Design and Subcloning of Recombinant Brain Spectrin Polypeptides. The boundaries of all repeats were defined by the SMART database (*22*). The design of all αII- and βII-spectrin single repeats and tandem-repeat fragments followed that for αI- and βI-spectrin fragments (*20*). The residue numbers of all sequences are given in Table 1. αIIR14, αIIR18, βIIR9, and βIIR11 were subcloned into the pET31b(+) vector, using *NSi*I and *Xho*I. All other brain spectrin single repeats and two-repeat fragments were subcloned into the pGEX-4T-2 vector, using *Eco*RI and *Sal*I restriction enzymes upstream and downstream, respectively. Three different αII-spectrin clones (*23*) and human brain cDNA were used to amplify the required αII repeats. For αIIR1, αIIR2, αIIR3, and αIIR4, the template was clone JS1. For αIIR5, αIIR6, αIIR7, and αIIR8, the template was Marathon cDNA. Clone 2.7A was used as a template to amplify αIIR9−10, αIIR11, αIIR12, and αIIR13. The template used to amplify the remaining αII-spectrin repeats was clone 3′DA. Similarly, three βII-spectrin clones (*24*) were used as templates to amplify βII-spectrin single repeats and tandem-repeat fragments. For βIIR1, βIIR2, βIIR3, βIIR4, βIIR5, βIIR6, βIIR7, and βIIR8, the template was β5.1, while for βIIR9 and βIIR10, it was clone β2.1. Clone β1.20 was the template for amplification of the remaining βII repeats. The fidelity of all the constructs was confirmed by DNA sequencing.

Generation of Linker Exchange Constructs. To define the five-amino acid linker region, we used ClustalW (*25*) to align the sequences of tandem-repeat fragments αIIR12−13, αIR12−13, αI3−4, βIIR12−13, βI12−13, and βI9−10 with the sequence of Protein Data Bank (PDB) entry 1S35. PDB entry 1S35 is tandem repeat βIR8−9, for which the heptad repeats and linker region have been defined (*26*). The replacement of αIIR12−13 linker GDSHD with the corresponding αIR12−13 linker NEAQK or αIR3−4 linker QATYW was accomplished by site-directed mutagenesis using the Stratagene QuickChange kit. The same method was used to replace βIIR12−13 linker EEAHR with βIR12−13 linker RDANE or βIR9−10 linker RDNLE. All the sequences were confirmed by DNA sequencing.

Preparation of Recombinant Polypeptides. The cDNA encoding the desired polypeptide was transformed into *Escherichia coli* BL21. The expression, thrombin cleavage to remove GST, and purification of the polypeptides were performed as described previously (*20*). The products were dialyzed against phosphate-buffered isotonic saline [buffer A being 10 mM sodium phosphate (pH 7.4) and 150 mM sodium chloride] and clarified before use by ultracentrifugation at 230000*g* for 30 min at 4 °C. Protein concentrations of the polypeptides were determined spectrophotometrically, using calculated specific absorptivities (*27*).

Mass Spectrometric Analysis and Sedimentation Equilibrium. Mass spectrometric analyses were performed using an Applied Biosystems (ABI, Foster City, CA) Voyager DE MALDI mass spectrometer. Spectrin polypeptide (2−10 μM) in low-salt solution was mixed with equal volume of a 10 mg/mL 3,5-dimethoxy-4-hydroxycinnamic acid solution (Sigma). One microliter of each mixture was spotted onto the MALDI plate. Spectra were calibrated against bovine serum albumin or myoglobin as an external standard. Sedimentation equilibrium of all products in isotonic buffer A was performed in a Beckman Coulter ProteomeLab XL-A analytical ultracentrifuge, as described before. The rotor speed was set at 20 000 rpm, and the equilibrium distributions were scanned at 280 nm. A good fit to a monodisperse ideal model was obtained in all cases.

Circular Dichroism Spectra and Thermal Unfolding. Far-UV CD[1] spectra and temperature-induced unfolding were

[1] Abbreviations: CD, circular dichroism; T_m (degrees Celsius), thermal denaturation midpoint.

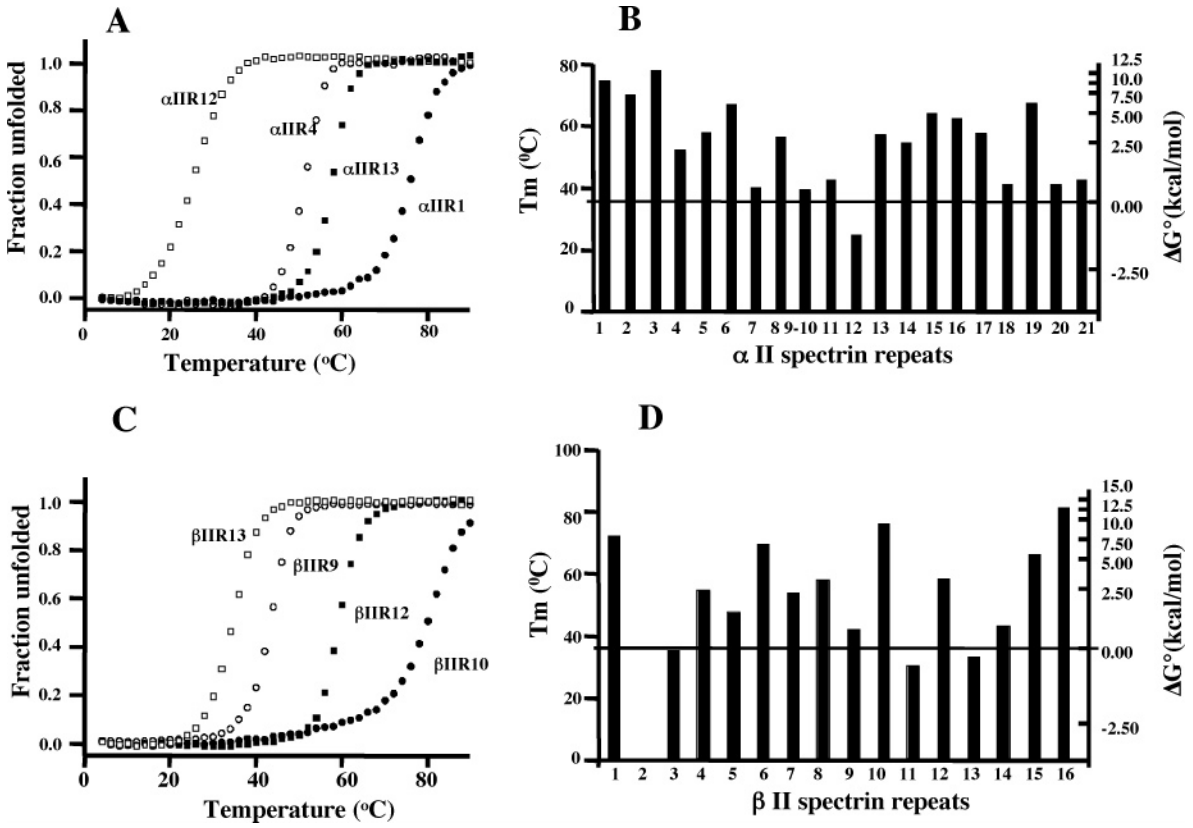

FIGURE 1: (A) Typical thermal unfolding profiles, measured by circular dichroism at 222 nm, corrected for linear changes above and below the sigmoidal unfolding transition, of expressed single repeats of αII-spectrin. The curves, from left to right, show unfolding of repeats 12, 4, 13, and 1. (B) T_m values of all repeats along the αII-spectrin chain. The horizontal line corresponds to the physiological temperature. The scale on the right shows the approximate free energy of unfolding of the repeats at 37 °C and applies also to the β-chain repeats in panel D. (C) Typical thermal unfolding profiles for single repeats of βII-spectrin, corrected as described above. The curves, from left to right, show unfolding of repeats 13, 9, 12, and 10. (D) T_m values of all repeats along the βII-spectrin chain.

performed as described previously (*20*). To determine the melting profiles, the ellipticity at 222 nm in buffer A was recorded at temperature intervals of 2 °C. The data were corrected for the linear changes above and below the sigmoid melting transition and expressed in terms of fraction unfolded. Coupling free energies, representing the conformational stabilization of one repeat in the tandem-repeat fragments by the other, were derived from van't Hoff plots of the corrected melting profiles of the isolated repeats and the lower-melting phases of those of the tandem repeats (*20*). The approximate free energy of unfolding of various single repeats at 37 °C was also calculated as described previously (*20*).

RESULTS

Recombinant αII- and βII-Spectrin Polypeptides. Table 1 lists the boundaries of the αII- and βII-spectrin repeats. The fragments, expressed as GST fusion constructs, contained six additional amino acids from the vector at their N-termini. Mass spectrometry confirmed that all had the expected molecular mass, and sedimentation equilibrium showed them to be monodisperse and monomeric in all cases. Circular dichroism spectra were characteristic of polypeptide chains with high α-helicity.

Temperature-Induced Unfolding of αII- and βII-Spectrin Single Repeats. We expressed and purified all αII- and βII-spectrin repeats and measured their thermal stabilities. All the repeats gave rise to typical sigmoidal unfolding equilibrium profiles, measured by the temperature dependence of circular dichroism at 222 nm. Panels A and C of Figure 1 show representative corrected unfolding profiles of αII- and βII-spectrin repeats, respectively. Panels B and D display the stability distribution of the repeats, in terms of the denaturation midpoints (T_m), along the αII- and βII-spectrin chains. These reveal appreciable differences from the corresponding results for erythrocyte spectrin (*20*). (1) Whereas eight of the 36 isolated repeats of the latter are more than 50% unfolded at physiological temperature, there are only four repeats of such low stability in αII/βII-spectrin. (2) While the T_m values of erythrocyte αI/βI-spectrin repeats lie between 21 and 72 °C, those of αII/βII-spectrin range from 25 to 81 °C (*3*). The T_m averaged over all isolated repeats is higher by some 10 °C in αII/βII- than in αI/βI-spectrin (55.5 and 46 °C, respectively). The relationship between the T_m and the approximate free energy of unfolding of the repeats at 37 °C is also shown in panels B and D of Figure 1. It is approximate only because the relation between T_m and $\Delta G°$ at the reference temperature (37 °C) is not fixed inasmuch as it varies with the enthalpy of the unfolding transition.

Temperature-Induced Unfolding of Tandem-Repeat Fragments. The thermal unfolding profiles of tandem-repeat fragments of erythrocyte spectrin demonstrated varying coupling, with stabilization of the less stable unit by the more stable unit (*20*); in all the cases that we examined, however, the biphasic character persisted, showing that cooperativity was by no means complete. Here we have examined the

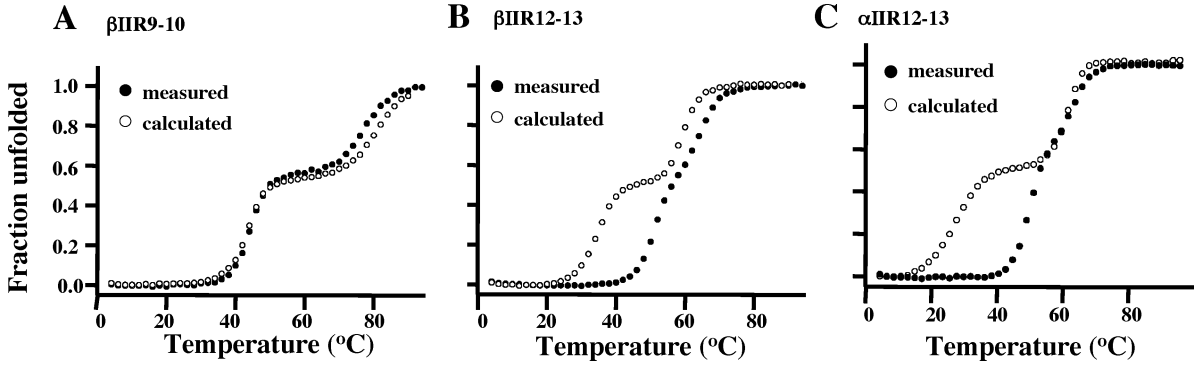

FIGURE 2: Thermal unfolding profiles of tandem-repeat constructs from αII and *β*II-spectrin chains. (A) Fragment comprising repeats 9 and 10 of *β*II-spectrin. (B) Fragment of repeats 12 and 13 of *β*II-spectrin. (C) Fragment of repeats 12 and 13 of αII-spectrin. All curves are corrected for linear slopes above and below the transition. Filled circles are observed data; empty circles are calculated for independent unfolding of the two repeats. Note the strong cooperativity of melting of the constituent repeats in panels B and C, while there is no perceptible coupling of the repeats in panel A.

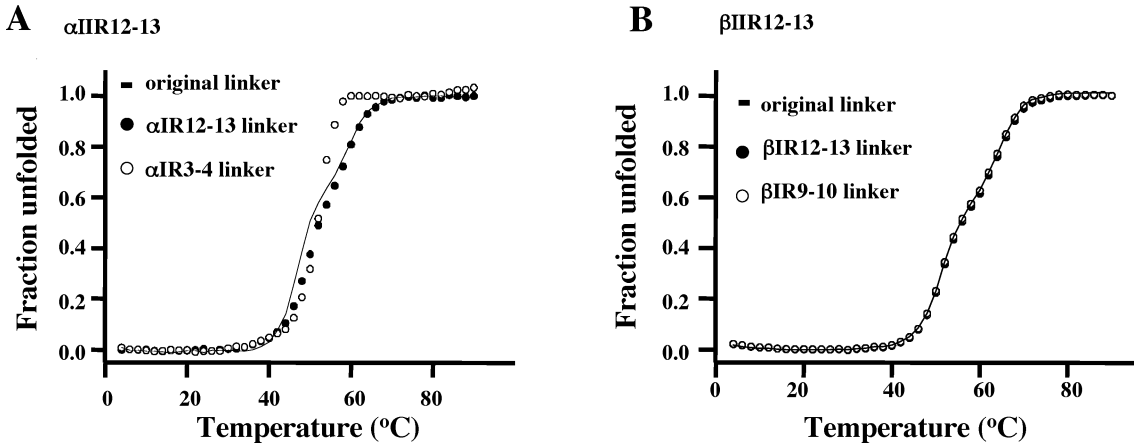

FIGURE 3: Thermal unfolding profiles of two-repeat fragments of brain spectrin with mutated linker regions. (A) Fragment comprising repeats 12 and 13 of the αII chain: wild type (—), substituent linker of αI-spectrin repeats 12 and 13 (●), and substituent linker of αI-spectrin repeats 3 and 4 (○). (B) Fragment comprising repeats 12 and 13 of the *β*II chain: wild type (—), substituent linker of *β*I-spectrin repeats 12 and 13 (●), and substituent linker of *β*I-spectrin repeats 9 and 10 (○). Note that in no case do the substitutions cause any perceptible loss of cooperativity.

unfolding of three tandem-repeat fragments of brain spectrin, αIIR12−13, *β*IIR9−10, and *β*IIR12−13. (Two additional such fragments, *β*IIR10−11 and *β*IIR11−12, were also prepared, but problems of aggregation vitiated the quality of the data, which we did not attempt to analyze.) The fragments were chosen to embody two folding units differing most widely in stability, as seen in Figure 1, and affording the best reflection therefore of cooperativity. As Figure 2 shows, the cooperativity is minimal in one of the fragments but large in the other two. Thus, in both *β*IIR12−13 (Figure 2B) and αIIR12−13 (Figure 2C), the conformation of the repeat of lower stability is substantially stabilized by interaction with its more stable neighbor (ΔT_m values of ca. 16 and 19 °C, respectively). The corresponding coupling free energies could be readily calculated as described previously (*20*), most usefully at the T_m of the less stable repeat in its isolated state (where its unfolding free energy is zero), and were found to be ca. −4.4 and −3.5 kcal/mol for *β*IIR12−13 and αIIR12−13, respectively. In the case of *β*II12−13 (Figure 3B), there is evidence (besides the large stabilization of the conformation of the less stable repeat) of a small but distinct stabilization of the more stable repeat by the attached unfolded repeat. This is not in itself remarkable and indeed has been reported before for a similar fragment (αII16−17) of chicken brain spectrin (*28*).

Contribution of the "Linker" Region to Cooperativity. MacDonald and Cummings (*29*) have inferred from secondary structure predictions by two methods that the α-helical propensities of sequences (linkers) of five residues at the center of the α-helix uniting adjacent repeats of erythrocyte spectrin govern the conformational stability of the tandem-repeat fragment. To determine whether the properties of the two tandem repeats (αIIR12−13 and *β*IIR12−13) that we have found to display strong cooperativity are affected by the nature of the linker, we prepared two mutants of each. In αIIR12−13, the sequence in question was replaced with the corresponding residues of αIR12−13 and of αIR3−4; in *β*IIR12−13, the linker residues were replaced with the analogous residues from *β*IR12−13 and *β*IR9−10. The substituents were chosen because all the erythrocyte spectrin tandem-repeat fragments from which they were derived display only weak to moderate cooperativity (*20*). As Figure 3A shows, the substitutions have relatively small effects on the unfolding profiles, although that of the erythroid αIR12−13 linker causes a discernible increase in stability, with no loss of cooperativity. The erythroid αIR3−4 linker engenders in addition a perceptible increase in cooperativity. Again (Figure 3B), the substitutions caused no major perturbation of the unfolding profiles of *β*II12−13.

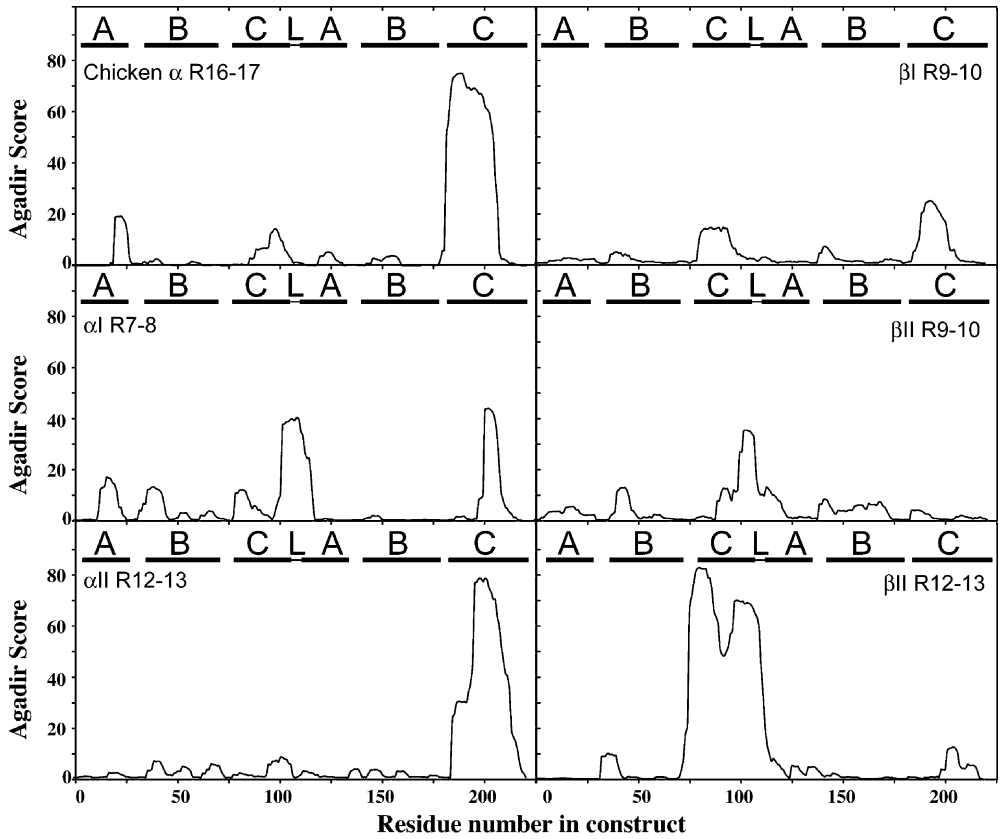

FIGURE 4: Agadir analysis of the helical propensity of triple-helical pairs. The figure shows predictions of helical propensity for the indicated paired spectrin repeats: chicken α-spectrin repeat 16−17 (from the sequence given in PDB entry 1U4Q), human αIR7−8, human αIIR12−13, human *β*IR9−10, human *β*IIR9−10, and human *β*IIR12−13. The sequence corresponding to helices A, B, and C of the repeats is indicated as well as the linker (L) sequence.

MacDonald and Cummings (*29*) suggested that the secondary structure of the linker regions dictates the stability of folding in pairs of adjacent repeats. They also noted a partial breakdown of cooperativity when the linker region was predicted not to be helical, but this was not a large effect, because in no cases, whether the denaturing agency was heat or urea, were separate melting phases observed. MacDonald and Cummings used for predictions first the DSC routine (*30*), which failed to predict correctly the structure of one linker that had been determined by crystallography, and second the PSIPRED routine (*31*), which delivered the correct answer. Since our data indicate that the relationship between cooperative coupling and linker sequence is more complex than the predictions of MacDonald and Cummings might suggest, we sought alternative means of investigating it. We made sequence alignments of highly cooperative and weakly cooperative pairs from multiple organisms, and we also ran predictions of the propensity of the sequences in the tandem pairs to form α-helices, using Agadir (*32*). Inspection of the multiple-sequence alignments disclosed no motifs or characteristic arrangement of types of amino acids that distinguished the different classes of pairs (Figure 4). Likewise, Agadir gave no consistent indication of the contribution of helical propensity either in the linker or in the helices that it joins.

At present, we cannot envisage any mechanism that might allow the linker to engender cooperative folding between repeats. Batey et al. (*28*) showed that mutations in the linker sequence can eliminate coupling. The only conclusion that seems compatible with all available data is that linkers between triple-helical repeats have evolved to allow or exclude cooperative coupling as required.

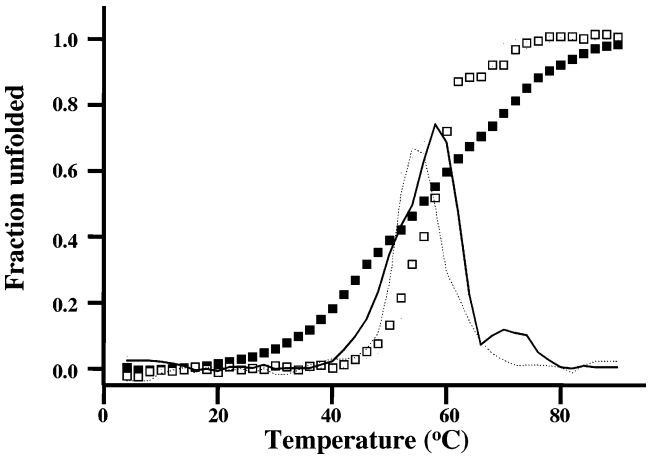

FIGURE 5: Thermal unfolding profile of intact αII*β*II-spectrin (□) and the summed melting profile of all single repeats (■). The first-order derivatives for αII*β*II-spectrin (—) and αI*β*I-spectrin (- - -) are also shown.

Intact Brain Spectrin. The denaturation profile of the pig brain spectrin tetramer is shown in Figure 5. This demonstrates, first, that there is extensive cooperative coupling between many of the repeats along the brain spectrin chains, since unfolding occurs much more sharply than would be calculated by merely summing the profiles of all individual repeats and, second, that the thermal stability of brain spectrin is greater than that of erythroid spectrin (T_m values of 49.5 and 58 °C, respectively). We have assumed that the result

for the brain spectrin tetramer will hold good also for the human protein, in view of the high degree of sequence conservation in mammalian species (*7*).

DISCUSSION

We have shown that the individual brain spectrin repeats, like those of erythroid spectrin, exhibit a wide range of thermal stabilities. The extent to which the low stability of certain repeats, such as αIIR12 and βIIR11, which are substantially unfolded at 37 °C (Figure 1), impacts the hydrodynamic flexibility of the intact protein remains uncertain as a consequence of the extensive (though varying) stabilizing interactions between successive repeats along the chain. Thus, the tandem-repeat construct, βIIR9−10, shows little interaction between its constituent parts, whereas in βIIR12−13, the free energy of coupling at the T_m of the isolated βIIR13 is some 4.4 kcal/mol. Even here, however, the shape of the unfolding profile indicates that cooperativity is incomplete, for the perceptible shoulder in the region of the midpoint reflects a significant weight of the half-unfolded form. This contrasts with the tandem repeat αIIR16−17 of chicken spectrin, which by this criterion exhibits completely cooperative melting (*28*). We cannot of course, on the basis of a circular dichroism profile alone, exclude small deviations from two-state behavior which, for instance, comparison with a fluorescence-based profile can reveal (*28*).

Law et al. (*33*, *34*) have demonstrated that some triple helices can be unfolded under physiological conditions by an applied pulling force, well within the range of the shearing forces encountered by the red cell in the circulation. Law et al. (*34*) have also shown that the magnitude of conformational coupling in forced unfolding diminishes with an increase in temperature. As an extreme example of this, the five-repeat fragment of erythrocyte spectrin βIR5−9 loses resistance to pulling in the atomic force microscope in two of its constituent repeats (R8−9) below 37 °C (*20*). The resulting local extension of a repeat to 4−5 times its folded length must be supposed to occur reversibly in red cells in the circulation.

Our data reveal major evolutionary adaptations between αI- and αII-spectrins. The αI-spectrin confers on the erythrocyte membrane the elasticity required for survival in the circulation. It has six repeats with a T_m at or below 37 °C (*20*). These repeats exhibit substantially incomplete conformational coupling with their neighbors. By contrast, αII-spectrin has only one repeat with a T_m below 37 °C, and this is conformationally coupled to R13 so that the αIIR12−13 pair has a T_m substantially higher than 37 °C.

What remains to be considered is the structural basis for the much greater stiffness of brain spectrin compared to erythroid spectrin, apparent from its hydrodynamic properties (*16*, *19*) and its appearance in the electron microscope (*16*−*19*). Figure 4 shows that brain spectrin also has the greater thermal stability, as previously observed by Di Stasi et al. (*35*) for bovine brain and erythrocyte spectrins, and also strong conformational coupling throughout. A high degree of stiffness could perhaps be related to the close lateral association between the αII- and βII-chains, apparent in electron microscope images of brain spectrin. Law et al. (*36*) have shown that lateral association [which in erythroid spectrin is confined to a run of four repeats in each chain at one end of the dimer (*37*)] promotes cooperative unfolding. Constructs of αII- and βII-spectrin, other than those containing the corresponding four repeats, show, like those of the αI- and βI-proteins (*38*), little interaction in vitro (unpublished data in this laboratory). At the same time, the greater average structural stability along the array of repeats in both brain spectrin chains, even if a few partly unfolded in the low-temperature range at the foot of the melting profile, must be expected to reduce the incidence of conformationally weak regions. The asymmetry apparent in the derivative curve in Figure 4 suggests that there is some clustering of stable and less stable repeats in the chains, and/or of regions in which cooperativity is greater or smaller. The data we have presented for the entire range of repeats should assist in the selection of chain elements for further study.

REFERENCES

1. Bennett, V., and Baines, A. J. (2001) Spectrin and ankyrin-based pathways: Metazoan inventions for integrating cells into tissues, *Physiol. Rev. 81*, 1353−92.
2. Pinder, J. C., and Baines, A. J. (2000) A protein accumulator, *Nature 406*, 253−4.
3. Yan, Y., Winograd, E., Viel, A., Cronin, T., Harrison, S. C., and Branton, D. (1993) Crystal structure of the repetitive segments of spectrin, *Science 262*, 2027−30.
4. Speicher, D. W., and Marchesi, V. T. (1984) Erythrocyte spectrin is comprised of many homologous triple helical segments, *Nature 311*, 177−80.
5. Kennedy, S. P., Warren, S. L., Forget, B. G., and Morrow, J. S. (1991) Ankyrin binds to the 15th repetitive unit of erythroid and nonerythroid β-spectrin, *J. Cell Biol. 115*, 267−77.
6. An, X., Guo, X., Sum, H., Morrow, J., Gratzer, W., and Mohandas, N. (2004) Phosphatidylserine binding sites in erythroid spectrin: Location and implications for membrane stability, *Biochemistry 43*, 310−5.
7. Salomao, M., An, X., Guo, X., Gratzer, W., Mohandas, N., and Baines, A. J. (2006) Mammalian α I-spectrin is a neofunctionalized polypeptide adapted to small, highly deformable erythrocytes, *Proc. Natl. Acad. Sci. U.S.A. 103*, 643−8.
8. Prchal, J. T., Papayannopoulou, T., and Yoon, S. H. (1990) Patterns of spectrin transcripts in erythroid and non-erythroid cells, *J. Cell. Physiol. 144*, 287−94.
9. Carlin, R. K., Bartelt, D. C., and Siekevitz, P. (1983) Identification of fodrin as a major calmodulin-binding protein in postsynaptic density preparations, *J. Cell Biol. 96*, 443−8.
10. Bennett, P. M., Baines, A. J., Lecomte, M. C., Maggs, A. M., and Pinder, J. C. (2004) Not just a plasma membrane protein: In cardiac muscle cells α-II spectrin also shows a close association with myofibrils, *J. Muscle Res. Cell Motil. 25*, 119−26.
11. Baines, A. J., and Pinder, J. C. (2005) The spectrin-associated cytoskeleton in mammalian heart, *Front. Biosci. 10*, 3020−33.
12. Moorthy, S., Chen, L., and Bennett, V. (2000) *Caenorhabditis elegans* β-G spectrin is dispensable for establishment of epithelial polarity, but essential for muscular and neuronal function, *J. Cell Biol. 149*, 915−30.
13. Hammarlund, M., Davis, W. S., and Jorgensen, E. M. (2000) Mutations in β-spectrin disrupt axon outgrowth and sarcomere structure, *J. Cell Biol. 149*, 931−42.
14. Knowles, W. J., Morrow, J. S., Speicher, D. W., Zarkowsky, H. S., Mohandas, N., Mentzer, W. C., Shohet, S. B., and Marchesi, V. T. (1983) Molecular and functional changes in spectrin from patients with hereditary pyropoikilocytosis, *J. Clin. Invest. 71*, 1867−77.
15. An, X., Lecomte, M. C., Chasis, J. A., Mohandas, N., and Gratzer, W. (2002) Shear-response of the spectrin dimer-tetramer equilibrium in the red blood cell membrane, *J. Biol. Chem. 277*, 31796−800.
16. Burridge, K., Kelly, T., and Mangeat, P. (1982) Nonerythrocyte spectrins: Actin-membrane attachment proteins occurring in many cell types, *J. Cell Biol. 95*, 478−86.
17. Bennett, V., Davis, J., and Fowler, W. E. (1982) Brain spectrin, a membrane-associated protein related in structure and function to erythrocyte spectrin, *Nature 299*, 126−31.

18. Glenney, J. R., Jr., Glenney, P., Osborn, M., and Weber, K. (1982) An F-actin- and calmodulin-binding protein from isolated intestinal brush borders has a morphology related to spectrin, *Cell 28*, 843−54.
19. Davis, J., and Bennett, V. (1983) Brain spectrin. Isolation of subunits and formation of hybrids with erythrocyte spectrin subunits, *J. Biol. Chem. 258*, 7757−66.
20. An, X., Guo, X., Zhang, X., Baines, A. J., Debnath, G., Moyo, D., Salomao, M., Bhasin, N., Johnson, C., Discher, D., Gratzer, W. B., and Mohandas, N. (2006) Conformational stabilities of the structural repeats of erythroid spectrin and their functional implications, *J. Biol. Chem. 281*, 10527−32.
21. Tyler, J. M., Hargreaves, W. R., and Branton, D. (1979) Purification of two spectrin-binding proteins: Biochemical and electron microscopic evidence for site-specific reassociation between spectrin and bands 2.1 and 4.1, *Proc. Natl. Acad. Sci. U.S.A. 76*, 5192−6.
22. Schultz, J., Milpetz, F., Bork, P., and Ponting, C. P. (1998) SMART, a simple modular architecture research tool: Identification of signaling domains, *Proc. Natl. Acad. Sci. U.S.A. 95*, 5857−64.
23. Moon, R. T., and McMahon, A. P. (1990) Generation of diversity in nonerythroid spectrins. Multiple polypeptides are predicted by sequence analysis of cDNAs encompassing the coding region of human nonerythroid α-spectrin, *J. Biol. Chem. 265*, 4427−33.
24. Hu, R. J., Watanabe, M., and Bennett, V. (1992) Characterization of human brain cDNA encoding the general isoform of *β*-spectrin, *J. Biol. Chem. 267*, 18715−22.
25. Higgins, D. G., and Sharp, P. M. (1988) CLUSTAL: A package for performing multiple sequence alignment on a microcomputer, *Gene 73*, 237−44.
26. Grum, V. L., Li, D., MacDonald, R. I., and Mondragon, A. (1999) Structures of two repeats of spectrin suggest models of flexibility, *Cell 98*, 523−35.
27. Perkins, S. J. (1986) Protein volumes and hydration effects. The calculations of partial specific volumes, neutron scattering matchpoints and 280-nm absorption coefficients for proteins and glycoproteins from amino acid sequences, *Eur. J. Biochem. 157*, 169−80.
28. Batey, S., Randles, L. G., Steward, A., and Clarke, J. (2005) Cooperative folding in a multi-domain protein, *J. Mol. Biol. 349*, 1045−59.
29. MacDonald, R. I., and Cummings, J. A. (2004) Stabilities of folding of clustered, two-repeat fragments of spectrin reveal a potential hinge in the human erythroid spectrin tetramer, *Proc. Natl. Acad. Sci. U.S.A. 101*, 1502−7.
30. King, R. D., and Sternberg, M. J. (1996) Identification and application of the concepts important for accurate and reliable protein secondary structure prediction, *Protein Sci. 5*, 2298−310.
31. Jones, D. T. (1999) Protein secondary structure prediction based on position-specific scoring matrices, *J. Mol. Biol. 292*, 195−202.
32. Munoz, V., and Serrano, L. (1997) Development of the multiple sequence approximation within the AGADIR model of α-helix formation: Comparison with Zimm-Bragg and Lifson-Roig formalisms, *Biopolymers 41*, 495−509.
33. Law, R., Carl, P., Harper, S., Dalhaimer, P., Speicher, D. W., and Discher, D. E. (2003) Cooperativity in forced unfolding of tandem spectrin repeats, *Biophys. J. 84*, 533−44.
34. Law, R., Liao, G., Harper, S., Yang, G., Speicher, D. W., and Discher, D. E. (2003) Pathway shifts and thermal softening in temperature-coupled forced unfolding of spectrin domains, *Biophys. J. 85*, 3286−93.
35. Di Stasi, A. M., Petrucci, T. C., and Minetti, M. (1987) Comparison of thermal properties of bovine spectrin and fodrin, *Arch. Biochem. Biophys. 256*, 144−9.
36. Law, R., Harper, S., Speicher, D. W., and Discher, D. E. (2004) Influence of lateral association on forced unfolding of antiparallel spectrin heterodimers, *J. Biol. Chem. 279*, 16410−6.
37. Ursitti, J. A., Kotula, L., DeSilva, T. M., Curtis, P. J., and Speicher, D. W. (1996) Mapping the human erythrocyte *β*-spectrin dimer initiation site using recombinant peptides and correlation of its phasing with the α-actinin dimer site, *J. Biol. Chem. 271*, 6636−44.
38. Speicher, D. W., Weglarz, L., and DeSilva, T. M. (1992) Properties of human red cell spectrin heterodimer (side-to-side) assembly and identification of an essential nucleation site, *J. Biol. Chem. 267*, 14775−82.

BI061368X